Atmos. Meas. Tech., 14, 6233–6247, 2021
https://doi.org/10.5194/amt-14-6233-2021

Atmospheric Measurement Techniques
Open Access
EGU

Tropospheric and stratospheric NO retrieved from ground-based Fourier-transform infrared (FTIR) measurements

Minqiang Zhou[1,2,3], Bavo Langerock[2], Corinne Vigouroux[2], Bart Dils[2], Christian Hermans[2], Nicolas Kumps[2], Weidong Nan[3], Jean-Marc Metzger[5], Emmanuel Mahieu[6], Ting Wang[1,3], Pucai Wang[1,3,4], and Martine De Mazière[2]

[1]CNRC & LAGEO, Institute of Atmospheric Physics, Chinese Academy of Sciences, Beijing, China
[2]Royal Belgian Institute for Space Aeronomy (BIRA-IASB), Brussels, Belgium
[3]Xianghe Observatory of Whole Atmosphere, Institute of Atmospheric Physics, Chinese Academy of Sciences, Xianghe, China
[4]CEPS, University of Chinese Academy of Sciences, Beijing, China
[5]UMS 3365 – OSU Réunion, Université de La Réunion, Saint-Denis, Réunion, France
[6]Institut d'Astrophysique et de Géophysique, UR SPHERES, Université de Liège, Liège, Belgium

Correspondence: Minqiang Zhou (minqiang.zhou@aeronomie.be, minqiang.zhou@mail.iap.ac.cn)

Received: 27 April 2021 – Discussion started: 5 May 2021
Revised: 10 August 2021 – Accepted: 10 August 2021 – Published: 28 September 2021

Abstract. Nitric oxide (NO) is a key active trace gas in the atmosphere, which contributes to form harmful ozone in the troposphere and to the destruction of ozone in the stratosphere. In this study, we present the NO retrieval from ground-based Fourier-transform infrared (FTIR) solar absorption spectrometry measurements at a polluted site (Xianghe, China) and a background site (Maïdo, Reunion Island). The degree of freedom (DOF) of the NO retrieval is 2.3 ± 0.4 (1σ) at Xianghe and 1.3 ± 0.1 at Maïdo.

By looking at the FTIR NO retrievals at Xianghe and Maïdo, we find that the stratospheric NO partial column is large in summer as compared to winter at both sites, and the seasonal variation in the FTIR stratospheric NO partial columns is consistent with that observed by the co-located Michelson Interferometer for Passive Atmospheric Sounding (MIPAS) satellite measurements. A large diurnal variation in the stratospheric NO partial column is observed by the FTIR measurements at Maïdo, with an increase from the early morning to about 14:00 local time and a decrease thereafter.

Due to the low NO concentration near the surface, the FTIR NO retrieval is only sensitive to the stratosphere at Maïdo. The high NO mole fraction near the surface at Xianghe allows us to derive tropospheric and stratospheric NO partial columns separately, although the tropospheric column is very difficult to retrieve in summer (June–August) because of the high water vapor abundance. A good correlation is found between the NO observed by the FTIR measurements and other air pollutants (NO_2 and CO) in the troposphere at Xianghe. It is the first study of a successful analysis of NO in the troposphere from a ground-based FTIR site. The tropospheric and stratospheric NO retrieval might be possible at other potential FTIR sites inside or near large cities with enhanced levels of NO near the surface.

1 Introduction

Nitric oxide (NO) is a major component of the nitrogen oxide family ($NO_x = NO + NO_2$), which plays key roles in atmospheric chemistry. In the troposphere, NO is an air pollutant, related to the formation of ground-level ozone (O_3), peroxyacetyl nitrate (PAN), nitric acid (HNO_3), and aerosols (Crutzen, 1979; Ng et al., 2007; Monks et al., 2015). NO sources near the surface are mainly of anthropogenic origin. Delmas et al. (1997) pointed out that about 50 % of the NO emissions are caused by the combustion of fossil fuel, and about 20 % are from the biomass burning. The remaining 30 % are mainly from natural lightning and microbial activity in soils. In the stratosphere, NO participates in an important set of catalytic reactions which deplete ozone (Crutzen, 1970). Stratospheric NO is mainly coming from

the oxidation of nitrous oxide (N_2O), which is a stable trace gas that can be transported upward to the stratosphere in the tropical region. As atmospheric N_2O has been increasing since the 1970s, mainly due to increasing use of fertilizers (Park et al., 2012), stratospheric ozone depletion caused by NO_x will play a more important role in the future, especially as the stratospheric chlorine burden is declining (Portmann et al., 2012). In the mesosphere and thermosphere, NO is formed by energetic particle precipitation (Randall et al., 2007), which can be transported downward to the stratosphere, affecting the ozone chemistry, especially in the winter polar region (Meraner and Schmidt, 2016).

Spaceborne sensors, e.g., the Atmospheric Chemistry Experiment–Fourier Transform Spectrometer (ACE–FTS) making solar occultation measurements (Bernath et al., 2005) and the Michelson Interferometer for Passive Atmospheric Sounding (MIPAS) looking at thermal emission at the limb (Fischer et al., 2008), can provide global NO distributions. However, these satellite measurements provide almost no information in the troposphere. Moreover, it is difficult to derive the diurnal variation in NO from these satellite measurements. Because of the weak intensities of the NO absorption lines (Gordon et al., 2017), as far as we know, there is no nadir-looking satellite to measure the NO near the surface. Ground-based Fourier-transform infrared (FTIR) spectrometers affiliated with the Network for Detection of Atmospheric Composition Change (NDACC) (De Mazière et al., 2018) record direct solar absorption spectra in the infrared region with a high spectral resolution (0.0035–0.005 cm^{-1}) under clear-sky conditions. More than 20 atmospheric species can be retrieved from the FTIR observed spectra, and the data have been widely used to investigate the change in atmospheric composition to support satellite validation and model verification (De Mazière et al., 2018). However, until now, there are few studies focusing on FTIR NO retrieval. Notholt et al. (1995) showed that the NO total columns can be retrieved from the FTIR spectra with a high spectral resolution of 0.0035 cm^{-1} at Ny-Ålesund. Wiacek et al. (2006) succeeded in retrieving NO in the stratosphere, mesosphere, and in the lower thermosphere from the ground-based FTIR measurements at Toronto and Eureka, but they found that there is almost no information in the troposphere for the FTIR NO retrievals at Eureka or even for measurements taken in the Toronto megacity.

In this study, we investigate NO retrievals from ground-based FTIR measurements with a focus on the retrieved profile in the troposphere and stratosphere at two different sites: Xianghe (a polluted site in China) and the Maïdo observatory on Reunion Island (a background site). The aims of this study are (1) to investigate whether it is possible to retrieve NO partial columns in the troposphere and stratosphere from the ground-based FTIR measurements, especially at the polluted site Xianghe, and (2) to understand the diurnal, synoptic, and/or seasonal variations in NO partial columns observed by the ground-based FTIR measurements in the stratosphere (and troposphere if possible) at Xianghe and Maïdo, together with other measurements, such as co-located satellite measurements. In Sect. 2, we give a brief introduction of the sites and the FTIR measurement technique and discuss the FTIR NO retrieval strategy and retrieval uncertainties. In Sect. 3, we discuss the time series of the FTIR NO retrievals at Xianghe and Maïdo, including the diurnal and seasonal variations in the FTIR-retrieved partial columns of NO in the stratosphere. In addition, the FTIR-NO-retrieved stratospheric partial columns are compared with the co-located MIPAS satellite measurements. Moreover, the FTIR-retrieved tropospheric partial columns of NO at Xianghe are discussed in Sect. 4. Finally, conclusions are summarized in Sect. 5.

2 Measurement sites and retrieval strategy

2.1 FTIR sites

- Xianghe (39.75° N, 116.96° E; 50 m a.s.l.) is located in a polluted urban region in North China. It is about 70 km southeast of Beijing. A Bruker IFS 125HR spectrometer was installed at Xianghe and started measuring infrared solar absorption spectra in June 2018 (Zhou et al., 2020). The Xianghe site is operated in the Total Column Carbon Observing Network (TCCON) mode by recording near-infrared spectra from 4000 to 12 000 cm^{-1} using an InGaAs detector (Yang et al., 2020), but infrared spectra with a spectral range from 1800 to 5200 cm^{-1} are also recorded with a liquid-N_2-cooled indium antimonide (InSb) detector. The spectra at Xianghe used for the NO retrieval are operated with the NDACC Infrared Working Group (IRWG) optical filter no. 5 (Blumenstock et al., 2021). The maximum optical path difference (MOPD) is 257 cm, which corresponds to a spectral resolution of 0.0035 cm^{-1}. There are normally one to five observed spectra on each measurement day. According to the Emissions Database for Global Atmospheric Research (EDGAR v4.3.2) (Crippa et al., 2018), the NO_x annual emission at Xianghe in 2012 is larger than 1000 $t\,yr^{-1}\,(0.1°)^{-2}$, which is one of the largest NO_x emission rates around the world. The NO concentration near the surface in this region was reported to be about 5–20 ppb (Tang et al., 2009). The high NO concentration provides an opportunity to study whether it is possible to retrieve tropospheric NO columns from the ground-based FTIR spectra.

- The Maïdo (21.08° S, 55.38° E; 2155 m a.s.l.) observatory, located on a mountain at Reunion Island, is about 700 km east of Madagascar in the Southern Hemisphere tropical region. The Bruker IFS 125HR spectrometer at Maïdo is affiliated with the NDACC IRWG (De Mazière et al., 2018) and has been measuring solar absorption spectra quasi-continuously since March 2013

(Zhou et al., 2016). The infrared spectra in the spectral range from 800 to 2000 cm^{-1} are recorded with a liquid-N_2-cooled mercury cadmium telluride (MCT) detector, and the infrared spectra in the spectral range from 2000 to 5200 cm^{-1} are recorded with a liquid-N_2-cooled InSb detector. The spectra at Maïdo used for the NO retrieval are also operated with the NDACC IRWG optical filter no. 5. Different from Xianghe, the spectra at Maïdo used for the NO retrieval are operated with two MOPDs of 120 and 257 cm, corresponding to spectral resolutions of 0.0072 and 0.0035 cm^{-1}, respectively. The short MOPD is operated with a large solar zenith angle (SZA) ($> 60°$) to reduce the uncertainty in the light path change. The long MOPD is operated with a small SZA. There are normally 1–10 spectra on each measurement day. Since NO is not among the baseline species in the NDACC IRWG network, it is the first time that we study the NO retrieval at the Maïdo site. As the NO_x surface concentration is low at Maïdo, with a typical value of 0.1–0.5 ppb (Rocco et al., 2020), it can be considered to be a background site as compared to Xianghe.

2.2 FTIR retrieval strategy

The SFIT4 v0.9.4.4 retrieval code, updated from SFIT2 (Pougatchev et al., 1995), based on the optimal estimation method (Rodgers, 2000) is applied to retrieve the NO profile from the infrared spectra observed at Xianghe and Maïdo. A line-by-line model has been implemented in the forward model of the SFIT4 code to calculate the transmittance at a given wavenumber range:

$$\boldsymbol{Y} = \boldsymbol{F}(\boldsymbol{x}, \boldsymbol{b}) + \boldsymbol{\varepsilon}, \tag{1}$$

where $\boldsymbol{Y}$ is the observed spectrum; $\boldsymbol{F}(\boldsymbol{x}, \boldsymbol{b})$ is the forward model, with the inputs from the retrieved parameters ($\boldsymbol{x}$) and non-retrieved model parameters ($\boldsymbol{b}$); and $\boldsymbol{\varepsilon}$ is the uncertainty. The pressure and temperature dependences of the line shape allow us to retrieve some pieces of vertical information of the target gas. The HITRAN2016 spectroscopy (Gordon et al., 2017) is used here, and the strongest NO absorption lines are distributed in the range between 1820 and 1930 cm^{-1}. In order to select the strong NO lines and to reduce the interference from other species, especially H_2O, several windows have been tested. We find that the NO absorption lines at 1900 cm^{-1} are the best choice for ground-based FTIR NO retrieval at Xianghe and Maïdo, which have also been used in the previous studies (Notholt et al., 1995; Wiacek et al., 2006). Figure 1 shows an example of the spectral fitting in the retrieval window at Xianghe. In order to reduce the influence of the interfering species, the column of CO_2 is retrieved simultaneously together with the profile retrieval of NO.

A cost function ($J(\boldsymbol{x})$) is created, and the STIT4 algorithm uses an iterative Levenberg–Marquardt method to look for the optimal $\boldsymbol{x}$ to minimize the $J(\boldsymbol{x})$.

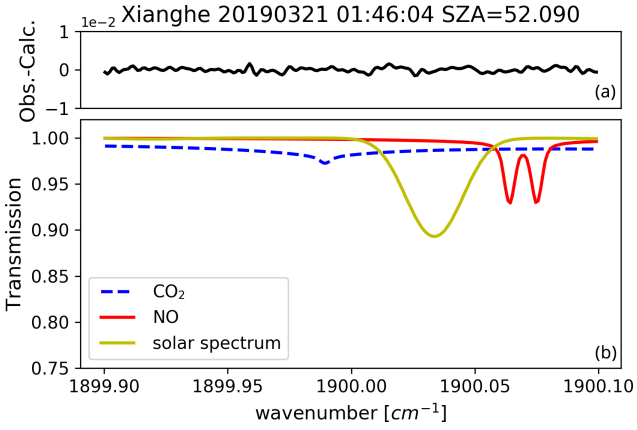

Figure 1. An example of the transmittances from NO, carbon dioxide (CO_2), and solar lines **(b)** and the difference between the observed and calculated spectra **(a)** in the NO retrieval window (1899.9–1900.1 cm^{-1}) at Xianghe. The measurement time (UTC) together with the solar zenith angle is shown in the title.

$$J(\boldsymbol{x}) = [\boldsymbol{y} - \boldsymbol{F}(\boldsymbol{x})]^T \mathbf{S}_{\boldsymbol{\epsilon}}^{-1} [\boldsymbol{y} - \boldsymbol{F}(\boldsymbol{x})] + [\boldsymbol{x} - \boldsymbol{x}_\mathrm{a}]^T \mathbf{S}_\mathrm{a}^{-1} [\boldsymbol{x} - \boldsymbol{x}_\mathrm{a}], \tag{2}$$

where $\mathbf{S}_\mathrm{a}$ is the a priori covariance matrix, and $\mathbf{S}_{\boldsymbol{\epsilon}}$ is the measurement covariance matrix. The retrieved state vector ($\boldsymbol{x}_\mathrm{r}$) can be written as

$$\boldsymbol{x}_r = \boldsymbol{x}_\mathrm{a} + \mathbf{A}(\boldsymbol{x}_\mathrm{t} - \boldsymbol{x}_\mathrm{a}) + \boldsymbol{\varepsilon}, \tag{3}$$

$$\mathbf{A} = (\mathbf{K}^T \mathbf{S}_{\boldsymbol{\epsilon}}^{-1} \mathbf{K} + \mathbf{S}_\mathrm{a}^{-1})^{-1} \mathbf{K}^T \mathbf{S}_{\boldsymbol{\epsilon}}^{-1} \mathbf{K}, \tag{4}$$

where $\boldsymbol{x}_\mathrm{a}$ and $\boldsymbol{x}_\mathrm{t}$ are the a priori and true state vectors (retrieved parameters), respectively; $\boldsymbol{\varepsilon}$ is the total error in the retrieved profile minus the smoothing error; $\mathbf{K}$ is the Jacobian matrix; and $\mathbf{A}$ is the averaging kernel (AVK), indicating the sensitivity of the retrieved parameters to the true parameters. A fixed a priori NO profile is used for all the retrievals at one site. The a priori profile of NO at Maïdo is derived from the average of the Whole Atmosphere Community Climate Model (WACCM) monthly means within 1980–2020 (Marsh et al., 2013), which is often used to create the a priori profile within the NDACC IRWG community. Note that the daytime and nighttime model data are both used in this case. There is an underestimation of NO near the surface from the WACCM model at Xianghe. The NO mole fraction is about 0.2 ppb in the WACCM model, while the surface observations in Beijing indicate that the NO mole fraction in this region is about 5–20 ppb near the surface during daytime (Tang et al., 2009). Therefore, we use the annual mean in 2018 from the Community Atmosphere Model with Chemistry (CAM-Chem) (Lamarque et al., 2012) monthly means as the a priori NO profile at Xianghe, with a NO mole fraction of 9.2 ppb at the surface. Since the top pressure level in the CAM-Chem

model is about 1.8 hPa (∼ 50 km), the a priori profile of NO at Xianghe above 50 km is taken from the WACCM model.

The regularization matrix for the NO retrieval is created with the Tikhonov $\mathbf{L}_1$ method (Tikhonov, 1963). $\mathbf{R} = \mathbf{S}_a^{-1} = \alpha \mathbf{L}_1^T \mathbf{L}_1$. To determine the value of α, we use the degree-of-freedom (DOF) method as described in Steck (2002). First, we create the a priori covariance matrix ($\mathbf{S}_a$) using the WACCM model monthly means. Second, the retrieval is operated using the optimal estimation method (OEM), and the DOF from the OEM is about 1.3 at Maïdo. Finally, we tune the α value to get a similar DOF using the Tikhonov method, implying $\alpha = 50$. In this study, we use the same α at both sites. The covariance matrix of the measurement ($\mathbf{S}_\epsilon$) is calculated as $1/\mathrm{SNR}^2$ for the diagonal values and 0 for the off-diagonal values. As a result, the AVK is affected by the signal-to-noise ratio (SNR) of the spectrum. Although there are only CO_2 and solar lines in our retrieval window, there are many strong water vapor lines adjacent to the window. Therefore, the SNR in this region is strongly affected by the water vapor abundance. The SNR is defined as the ratio of the maximum intensity of the spectra in the NO retrieval window to the root mean square error of the spectra in the noise window between 1650 and 1700 cm^{-1}. Figure 2 shows several typical spectra observed in summer and winter at Xianghe and Maïdo. According to the National Centers for Atmospheric Prediction (NCEP) reanalysis data (Kalnay et al., 1996), the mean total columns of H_2O are 3.8×10^{22} molecules cm^{-2} (7.5×10^{22} molecules cm^{-2} in summer and 1.6×10^{22} molecules cm^{-2} in winter) at Xianghe and 2.6×10^{22} molecules cm^{-2} (3.8×10^{22} molecules cm^{-2} in summer and 1.0×10^{22} molecules cm^{-2} in winter) at Maïdo. The H_2O interference is more important at Xianghe as compared to Maïdo. As a result, the SNR of the spectrum is less than 50 in summer and about 500 in winter at Xianghe, and it is about 200 in summer and about 700 in winter at Maïdo. HBr cell measurements are operated at both sites. The instrument line shape (ILS) parameters are retrieved from the cell measurements by the LINEFIT14.5 algorithm (Hase et al., 1999), and the LINEFIT outputs are used as the ILS inputs in the SFIT4 algorithm. The solar line list is included in the SFIT4 code, named 120621_solar, and the solar line intensity and shift are retrieved simultaneously in the NO retrieval. Table 1 summarizes the NO retrieval strategy used in this study.

Figure 3 shows the a priori and retrieved NO profiles in the vertical range between the surface and 70 km, together with typical AVKs at Xianghe and Maïdo, respectively. At both sites, the maximum value of the NO mole fraction occurs at about 45 km in the stratosphere. The retrieved NO mole fraction is much larger than the a priori in the stratosphere at both sites. The a priori NO profile is created as the average of the model monthly means including both daytime and nighttime data, while the NO mole fraction in the stratosphere at night is several orders of magnitude less than that during the daytime (Kondo et al., 1990; Dubé et al., 2020). Therefore, in the stratosphere the FTIR retrievals during the daytime are much larger than the a priori profile. The retrieved NO mole fraction near the surface is about 10 ppb at Xianghe, which is comparable to the observations in Beijing of 5–20 ppb during daytime (Tang et al., 2009). The NO mole fraction near the surface is about 0.01 ppb at Maïdo. The AVK at Xianghe shows that only the layers below 2 km have sensitivity near the surface, while other layers are mainly sensitive to the stratosphere. The AVK at Maïdo shows that the kernels of the troposphere and stratosphere both peak at the stratosphere (∼ 35 km), indicating that there is almost no information in the lower troposphere. According to the NCEP data, the mean tropopause heights at Xianghe and Maïdo are about 12 and 16 km, respectively. In this study, we take the vertical range between the surface and the tropopause height (12 km at Xianghe and 16 km at Maïdo) as the troposphere and the vertical range between the tropopause height and 60 km as the stratosphere.

Table 1. The retrieval strategy of FTIR NO retrieval in this study.

Parameter	Setting
Retrieval window	1899.90–1900.10 cm^{-1}
Profile retrieval	NO
Column retrieval	CO_2
A priori profile	WACCM (+ CAM-Chem at Xianghe)
Spectroscopy	HITRAN2016
Regularization	Tikhonov ($\alpha = 50$)
SNR	Calculated from the spectra
ILS	LINEFIT retrievals
Solar lines	The intensity and shift are retrieved

The trace of the AVK matrix is the degree of freedom (DOF) for signal, indicating the number of individual pieces of information. The mean DOFs of the retrieved NO profiles over the entire datasets are 2.3 ± 0.4 (1σ) at Xianghe and 1.3 ± 0.1 at Maïdo, respectively. Figure 4 shows the time series of the DOF in the troposphere, stratosphere, and above 60 km between July 2018 and June 2020 at Xianghe and between March 2013 and December 2019 at Maïdo. The DOF in the vertical range above 60 km is 0.20 ± 0.06 at Xianghe and 0.10 ± 0.02 at Maïdo. The DOF in the stratosphere is generally between 1.0 and 1.8 at both sites. The DOF in the troposphere is 0.78 ± 0.18, with 90 % of DOF from the layers below 2 km at Xianghe, reflecting that the tropospheric NO partial column is actually dominated by the NO partial column in the boundary layer. At Maïdo, the DOF in the troposphere is only 0.03 ± 0.02. In the remainder of this study, we consider only the measurements with a tropospheric DOF larger than 0.5 (dashed black line in Fig. 4) as the information on the tropospheric NO partial column will in this case come mostly from the retrieval and not from the a priori. In total, 472 out of 539 retrievals are selected, with almost none in summer (June to August). As seen in Fig. 4, there is a large seasonal variation in the DOF. The DOF is determined by the

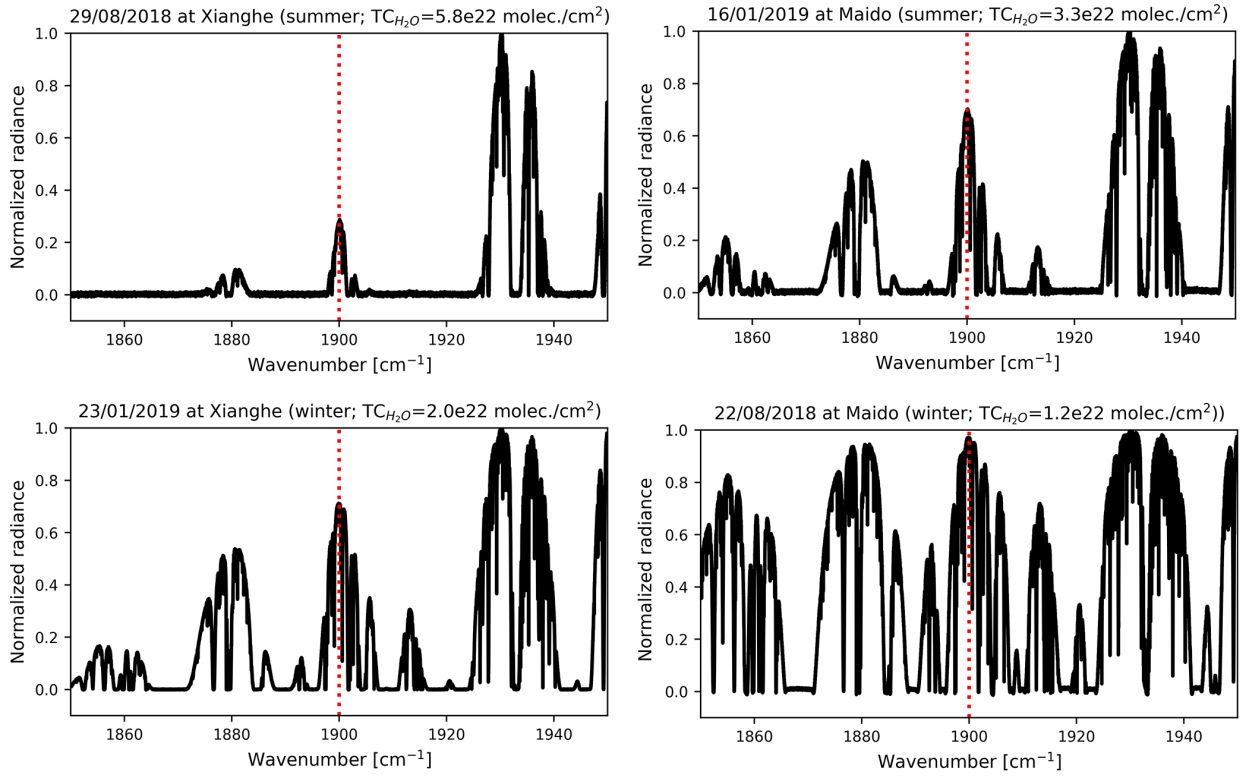

Figure 2. The normalized spectra in summer and winter at Xianghe and Maïdo, together with the total column of water vapor on these days. The dashed red line indicates the retrieval window for NO.

SNR of the spectrum, which is highly related to the H_2O total column (Fig. 5). A large H_2O abundance makes the signal in the selected spectral region weak, leading to a low DOF. The correlation coefficient (R) between DOF and H_2O total column is -0.88. Based on the linear fit, the FTIR NO retrievals at Xianghe with DOF in the troposphere larger than 0.5 are generally occurring when the H_2O total column is less than 5.7×10^{22} molecules cm^{-2}. In summary, we cannot retrieve NO in the troposphere at Maïdo because the NO mole fraction near the surface (NO_{surf}) is low, with a typical value of less than 0.1 ppb. At Xianghe, the spectra recorded under a wet condition (mainly occurring in summer) do not allow us to retrieve the tropospheric NO either. In winter, all the retrievals at Xianghe provide both tropospheric and stratospheric NO partial columns (Figs. 4 and 5). The retrieved NO_{surf} in winter ranges from 1.3 to 47.2 ppb, with a mean of 11.4 ppb and a standard deviation (SD) of 10.7 ppb. For all the 240 retrievals in winter, the mean of the H_2O total column is 2.3×10^{22} molecules cm^{-2}, and the mean of the SZA is 65.3°. A relatively lower NO_{surf} at Xianghe can be detected under the condition of a low H_2O total column and a large SZA. For example, if we only select the retrievals with the NO_{surf} less than 3 ppb (26 out of 240), the mean of the H_2O total column becomes 1.7×10^{22} molecules cm^{-2}, and the mean of the SZA is 68.1°.

Table 2 lists the systematic and random retrieval uncertainties in the NO total column at Xianghe and Maïdo, including the contributions from the major uncertainty sources, which are estimated based on the optimal estimation method (Rodgers, 2000). It is assumed that the systematic uncertainty in a priori profile is 10 %, and the random uncertainty in a priori profile is calculated from the covariance matrix of the monthly a priori profiles in 2018. The measurement error matrix is created by the SNR of the spectra so that each individual spectrum has a different measurement uncertainty matrix. The temperature systematic and random uncertainties are derived from the mean and SD of the differences between the NCEP and ECMWF reanalysis data. We set the systematic uncertainty in the NO spectroscopy to 10 % according to the HITRAN2016 line list (Gordon et al., 2017) and assume that there is no random uncertainty for the spectroscopy. The systematic and random uncertainties in SZAs are set to 0.1 % and 0.5 %, respectively. The retrieved parameter contains the interfering species (CO_2), the solar line intensity and shift, and the slope. The systematic and random uncertainties in CO_2 are set to 5 % and 10 %, respectively. We set 0.1 %, 1.0 %, and 0.5 % to both the random and systematic uncertainties in the slope, the solar line intensity and the solar line shift, respectively. In total, the systematic uncertainties in the FTIR-NO-retrieved total columns are simi-

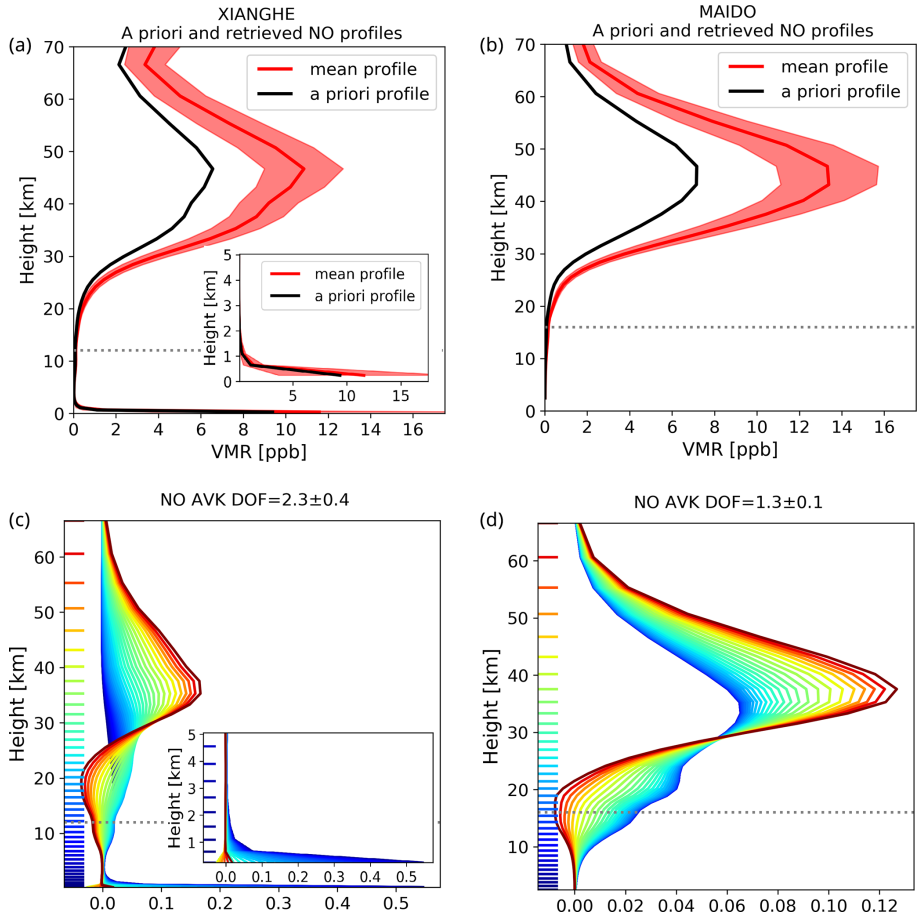

Figure 3. The a priori and retrieved NO profiles at Xianghe and Maïdo (upper panels), together with a typical averaging kernel (AVK) at each site (bottom panels). To better visualize the change near the surface, a zoom on the vertical range between 0 and 5 km is also shown for Xianghe. The red shadow in the upper panels is the standard deviation of the retrieved profiles. The dashed line indicates the tropopause height.

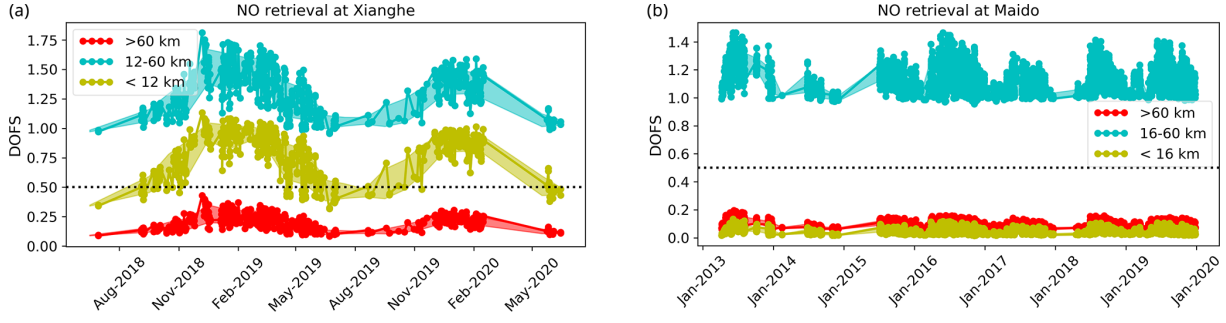

Figure 4. The series of the DOF daily mean (dots) and the SD (shadow) in the troposphere, stratosphere, and above at Xianghe **(a)** and Maïdo **(b)**. The dashed black line is at DOF of 0.5.

lar at Xianghe and Maïdo (∼ 10.3 %) and dominated by the uncertainty in the spectroscopy. The random uncertainty in retrieved NO total column is estimated to be 13.5 % at Xianghe, which is larger than that of 4.2 % at Maïdo. The random uncertainty is mainly coming from the smoothing error and the measurement uncertainty, where the large smoothing error at Xianghe is large due to the strong NO variation near the surface, and the large measurement uncertainty at Xianghe is coming from the low SNR of the spectra. At Maïdo, the systematic uncertainties in NO stratospheric partial column and total column are similar. The random uncertainty in NO stratospheric partial column is less than the ran-

Table 2. The retrieval uncertainties in the NO total and partial columns at Xianghe and Maïdo. All uncertainties are in percent (%).

Site	Xianghe						Maïdo			
	Total column		Troposphere (0–12 km)		Stratosphere (12–60 km)		Total column		Stratosphere (16–60 km)	
	Systematic	Random	Systematic	Random	Systematic	Random	Systematic	Random	Systematic	Random
Smoothing	1.5	12.0	1.7	16.2	1.5	2.4	0.2	3.6	0.1	1.5
Measurement	–	6.0	–	7.5	–	2.5	–	1.7	–	1.4
Retrieved parameters	1.2	1.2	1.1	1.1	1.5	1.5	0.4	0.4	0.5	0.5
Temperature	1.4	0.6	1.5	1.2	2.8	1.5	2.5	0.5	2.6	0.6
Spectroscopy	10.1	–	10.2	–	9.8	–	10.0	–	9.9	–
Solar zenith angle	0.3	1.5	0.4	1.8	0.3	1.6	0.2	1.0	0.2	1.0
Total	10.3	13.5	10.5	18.0	10.2	4.4	10.3	4.2	10.2	2.4

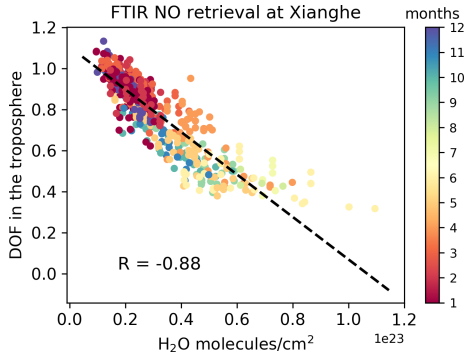

Figure 5. The scatterplots between the DOF in the troposphere and the H_2O total columns from the NCEP data, colored with the measurement month. The dashed black line is the linear fit, and R is the correlation coefficient.

dom uncertainty in NO total column, mainly due to a smaller smoothing error. At Xianghe, the systematic and random uncertainties in the NO partial columns in the troposphere and stratosphere are also shown in Table 2. The systematic and random uncertainties in the stratospheric NO partial column are 10.2 % and 4.4 %, respectively. The systematic and random uncertainties in the tropospheric NO partial column are 10.5 % and 18.0 %, respectively. The random uncertainty in the tropospheric NO partial column is larger as compared to the stratospheric partial column, and it is mainly coming from the smoothing error and the measurement uncertainty.

3 Stratospheric NO partial column

3.1 Diurnal variation

Due to photochemical reactions (Kondo et al., 1990), a large diurnal variation in the stratospheric NO concentration is expected. Figure 6 shows diurnal variations in stratospheric NO partial columns in all months at Maïdo, together with the SZA of the measurements. The stratospheric NO partial columns are fitted with a second-order polynomial fitting ($y(t) = a + bt + ct^2$; t is a fraction of local hour). No fitting is applied at Xianghe due to the lack of measurements, especially before 09:00 and after 16:00 LT. Note that the fitted line is also plotted at hours with no measurements, but it does not represent the physical reality due to the absence of data.

At Maïdo, the measurement often starts at 07:00 and stops at 17:30 LT. The FTIR measurements show that the stratospheric NO partial column increases with time until about 14:00 LT, and it starts decreasing afterwards. The decrease in NO after 14:00 LT indicates that more NO is converted to nitrogen dioxide (NO_2) than the NO formed from NO_2 at that time. This type of diurnal variation is consistent throughout the whole year at Maïdo. Based on the second-order polynomial fittings, it is found that the maximum stratospheric NO partial column occurs at 14.3 ± 0.4 h, which is 1.9 ± 0.6 h after the time of the minimum of the SZA (about 12:20 LT). There is almost no cloud in the stratosphere, so the solar radiation intensity is directly proportional to cos(SZA). The stratospheric NO partial columns increase with time in the morning, and we find that there is a good linear relationship between the stratospheric NO partial column and the solar radiation intensity (cos(SZA)) between 06:00 and 12:20 LT (Fig. 7), with an R of 0.80 at Xianghe and 0.74 at Maïdo. The fitted slope at Xianghe is $2.01 \pm 0.16 \times 10^{15}$, which is close to the slope of $1.87 \pm 0.12 \times 10^{15}$ at Maïdo. The FTIR measurements show that the speed of the formation of stratospheric NO in the morning at Maïdo is similar to that at Xianghe.

3.2 Time series and seasonal variation

Figure 8 shows the time series of the FTIR-NO-retrieved partial columns in the stratosphere at Xianghe and Maïdo. In order to derive the seasonal variation, the daily means $\boldsymbol{y}(t)$ are fitted by a periodic function

$$\boldsymbol{y}(t) = A_0 + A_1 \boldsymbol{t} + \sum_{k=1}^{3} (A_{2k} \cos(2k\pi \boldsymbol{t}) + A_{2k+1} \sin(2k\pi \boldsymbol{t})), \quad (5)$$

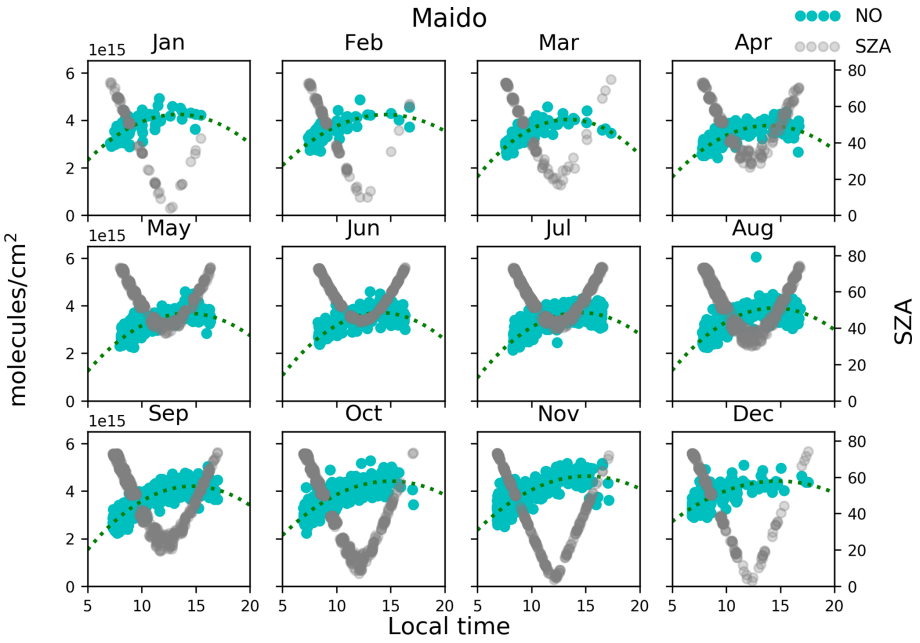

Figure 6. The diurnal variation in stratospheric NO partial column at Maïdo, together with the solar zenith angle (gray dots). The stratospheric NO partial columns are fitted with a second-order polynomial fitting (dotted cyan line).

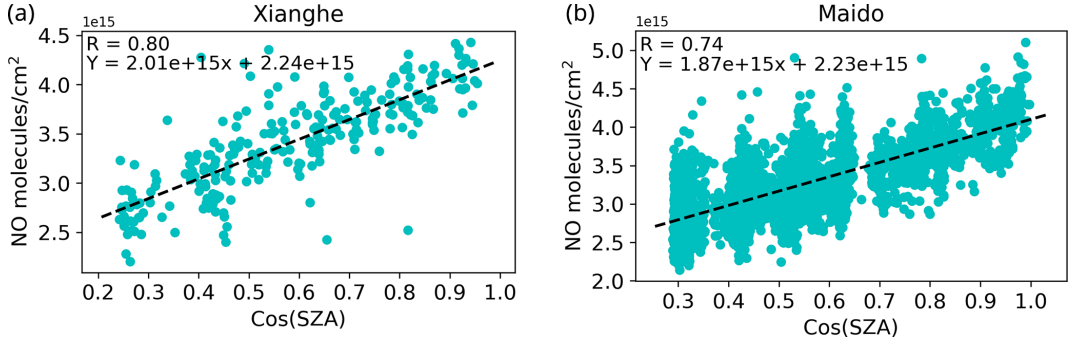

Figure 7. The correlation between the stratospheric NO partial column and the solar radiation (cos(SZA)) before 12:20 LT at Xianghe **(a)** and Maïdo **(b)**, respectively. R is the correlation coefficient, N is the measurement number, and the dashed black line is the linear fitting.

where $\boldsymbol{t}$ is the measurement time in units of fraction of a year; A_0 is the offset; A_1 is the long-term trend; and A_2 to A_7 are the periodic amplitudes, representing the seasonal variation. The annual relative change in units of $\%\,y^{-1}$ is relative to the mean of data used in the trend analysis. The daily means are calculated from only the measurements between 13:30 and 14:30 LT. The 1 h time window around the maximum of the tropospheric NO partial column is used to reduce the impact of the large diurnal variation in the stratospheric NO partial column as we found in Sect. 3.1. Since the time coverage is relatively short at Xianghe, we assume that there is no long-term trend ($A_1 = 0$).

The mean and SD of the stratospheric NO partial columns between 13:30 and 14:30 LT are $3.6 \pm 0.5 \times 10^{13}$ molecules cm^{-2} at Xianghe and $4.0 \pm 0.4 \times 10^{13}$ molecules cm^{-2} at Maïdo, respectively. The mean of the stratospheric partial columns at Maïdo is larger than that at Xianghe. The seasonal variation in NO is determined by the equilibrium between NO and NO_2 (NO_x) on the one hand and the reservoir substances, such as N_2O_5, HNO_3, and $ClONO_2$, on the other hand (Jacob, 1999; Vaughan et al., 2006). The FTIR measurements show that the stratospheric NO partial column is high in summer and low in winter, with a peak-to-peak amplitude of 1.1×10^{15} molecules cm^{-2} at Xianghe and 0.8×10^{15} molecules cm^{-2} at Maïdo. Keep in mind that the summer at Maïdo is December–February as it is located in the Southern Hemisphere.

The decrease in the stratospheric NO partial columns between 2013 and 2019 at Maïdo is observed by the FTIR measurements ($-0.42 \pm 0.57\,\%\,yr^{-1}$), although the decrease is insignificant as the annual change is within the uncertainty. Galytska et al. (2019) observed a significant decrease

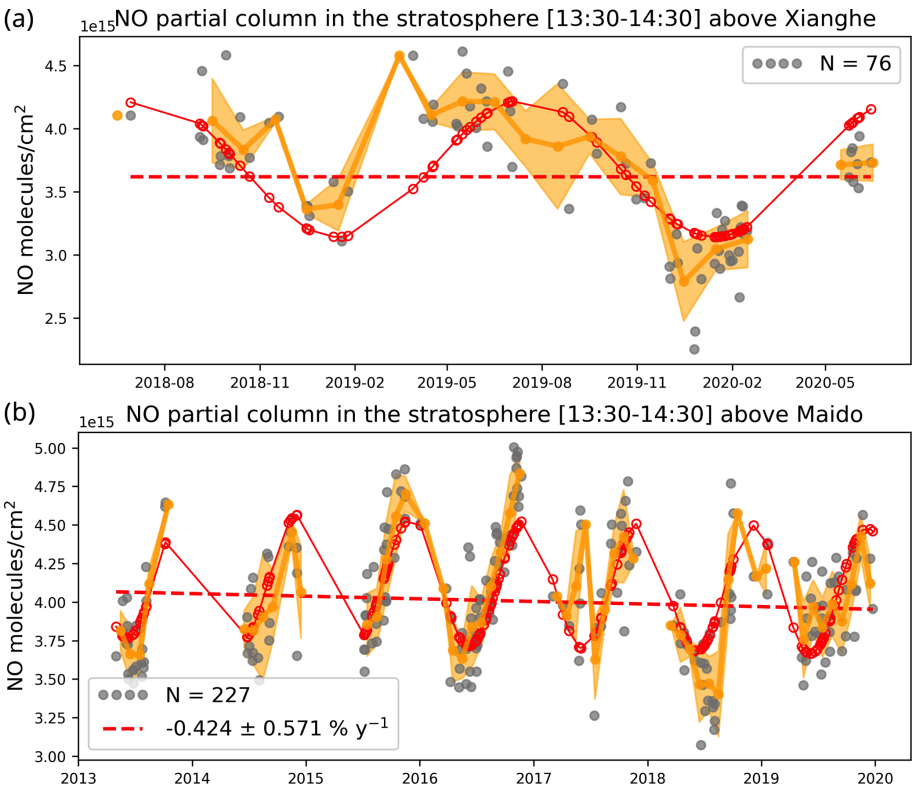

Figure 8. The time series of the FTIR-NO-retrieved stratospheric partial column daily means (gray dots) and monthly means and SDs (yellow dots and shadow) at Xianghe **(a)** and Maïdo **(b)** for only the measurements between 13:30 and 14:30 LT. N is the measurement days. The dashed red line is the $A_0 + A_1 t$ in Eq. (3), the red dots and the red solid line are the fittings with the seasonal variation.

in NO_2 from the SCIAMACHY satellite measurements in the Southern Hemisphere between 2002 and 2012, and Dubé et al. (2020) also found a negative NO_x trend in the Southern Hemisphere derived from SAGE II-OSIRIS satellite measurements and the WACCM model from 2005 to 2014. Although the time coverages of the FTIR measurements at Maïdo and the two previous studies are not the same, all these studies show a consistent negative trend in NO_x in the stratosphere at the latitude of Maïdo.

3.3 Comparison with MIPAS measurements

The MIPAS satellite observed the atmospheric NO concentrations globally between 2002 and 2012. There are two spectral resolutions for the MIPAS spectra: 0.05 cm^{-1} before January 2005, named full-spectral-resolution (FR) mode, and 0.121 cm^{-1} after January 2005, named reduced-resolution (RR) mode. In this study, we only use the NO MIPAS data after 2005, and the versions are V5r_NO_220 and V5r_NO_221. As MIPAS has a limb view, the MIPAS only provides the NO profile above $\sim$ 10 km. The NO profile is retrieved from MIPAS spectra at 5.3 µm (Bermejo-Pantaleón et al., 2011). The vertical resolution of the NO profile is about 4–6 km, and the uncertainty in the NO profile in the altitude range of 20–60 km is 5 %–40 % (Sheese et al., 2016).

There are no overlap MIPAS measurements with the FTIR measurements as Xianghe and Maïdo FTIR both started measuring after 2012. The MIPAS satellite has two windows overpassing one location (around 10:30 and 22:30 LT). The NO stratospheric partial column observed by MIPAS during the night (22:30 LT) is about 1×10^5 times less than that observed during the day (10:30 LT). In this section, we select all the MIPAS measurements between 2005 and 2012 within $\pm 2°$ latitude and $\pm 2°$ longitude around each FTIR site and only use the daytime-overpass measurements to compare with FTIR measurements. To take the vertical sensitivity of the FTIR retrieval into account, the MIPAS NO vertical profile is smoothed with the FTIR AVK (Rodgers and Connor, 2003). To reduce the influence from the diurnal variation in the stratospheric NO partial columns (Fig. 6), the FTIR measurements used to compare with MIPAS measurement are limited to the measurements between 09:30 and 11:30 LT.

Figure 9 shows the time series of the stratospheric NO partial columns observed by FTIR and MIPAS measurements above Xianghe and Maïdo. The seasonal variations in the stratospheric NO partial columns observed by MIPAS and FTIR measurements are similar, with a high value in summer and a low value in winter. The amplitudes of the seasonal variations of the stratospheric NO partial columns above Xianghe and Maïdo observed by the MIAPS measure-

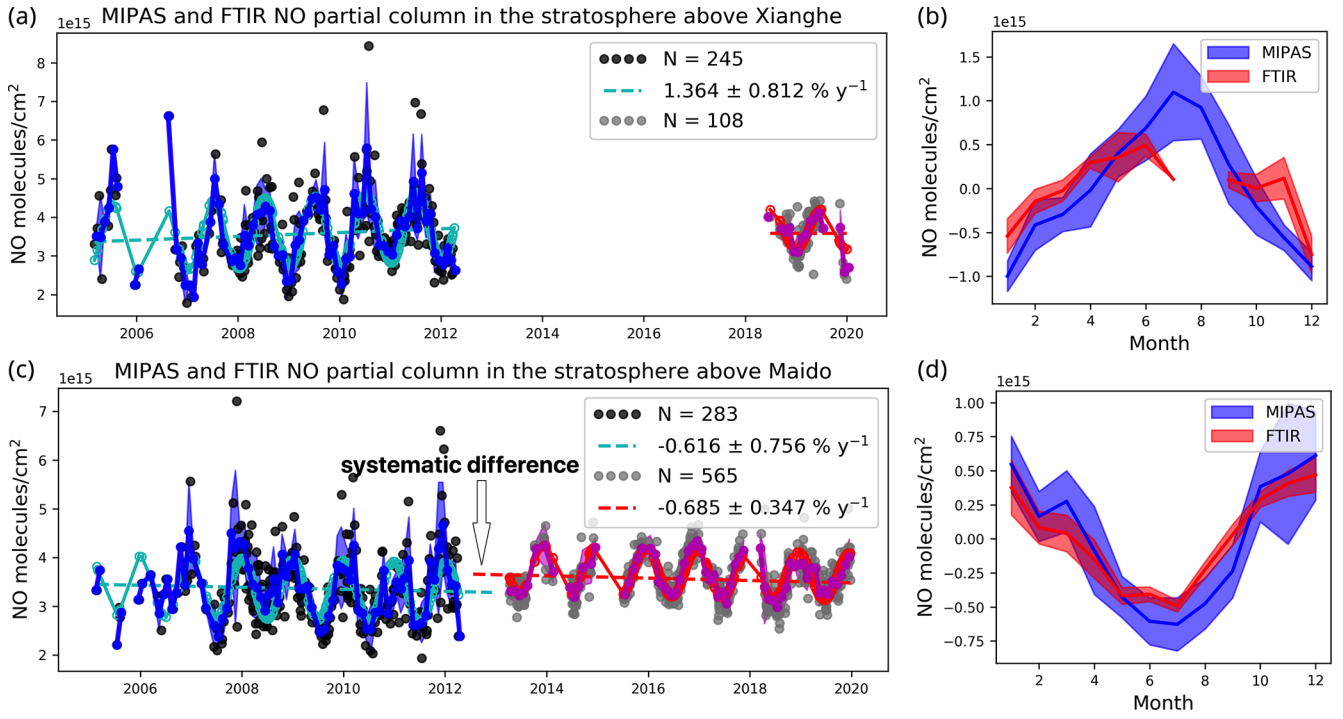

Figure 9. (a, c) The time series of the stratospheric NO partial columns observed by MIPAS measurements (black dots: daily means; solid blue line: monthly mean; blue shadow: monthly SD; dashed cyan line: trend fitting) and FTIR measurements (gray dots: daily means; solid purple line: monthly mean; purple shadow: monthly SD; dashed red line: trend fitting) above Xianghe **(a, b)** and Maïdo **(c, d)**. **(b, d)** The seasonal variations in the stratospheric NO partial columns observed by MIPAS measurements. The MIPAS measurements are selected within ±2° latitude and ±2° longitude around the sites. Numbers of the measurement days (N) are 245 and 283 from MIPAS at Xianghe and Maïdo, respectively. The FTIR measurements are selected with the measurement time between 09:30 and 11:30 LT, with 108 and 565 d at Xianghe and Maïdo, respectively. The annual changes in NO partial columns are derived from MIPAS measurements at Xianghe and Maïdo in 2005–2012 and from the FTIR measurements at Maïdo in 2013–2019. A systematic difference is detected between the MIPAS and FTIR NO stratospheric partial columns.

ments are 1.65×10^{15} and 1.19×10^{15} molecules cm^{-2}, respectively, which are larger than those observed by the FTIR measurements of 1.13×10^{15} molecules cm^{-2} above Xianghe and 1.09×10^{15} molecules cm^{-2} above Maïdo. The possible reason for this difference is that the retrieval uncertainty is relatively large for MIPAS measurements as we see many large values above both sites. The uncertainties in the MIPAS stratospheric NO partial column are 20.5 % and 24.7 % above Xianghe and Maïdo, respectively.

The MIPAS measurements show that stratospheric NO was increasing above Xianghe and decreasing above Maïdo between 2005 and 2014, which is consistent with the negative NO_x trends in the Southern Hemisphere and the positive NO_x trends in the Northern Hemisphere observed by SAGE II-OSIRIS satellite measurements between 2005 and 2014 (Dubé et al., 2020). Above Xianghe, it is impossible to derive the long-term trend from the FTIR measurements because of the limited measurements. Above Maïdo, the annual relative change in stratospheric NO partial columns observed by MIPAS measurements between 2005 and 2012 is -0.62 ± 0.77 % yr^{-1}, which is close to that of -0.68 ± 0.36 % yr^{-1} observed by the FTIR measurements between 2013 and 2019. However, we observe a systematic difference of 0.35×10^{15} molecules cm^{-2} between MIPAS and FTIR measurements, which corresponds to 10.6 % relative to MIPAS data and 9.6 % relative to FTIR measurements. The difference is within the uncertainties in both the MIPAS and FTIR measurements.

4 Tropospheric NO partial column

In this section, we only use the tropospheric NO partial columns retrieved by the FTIR measurements with a DOF larger than 0.5 in the troposphere at Xianghe. Figure 10 shows the scatterplots between the tropospheric NO partial columns and stratospheric NO partial columns. When the DOF is larger than 0.5 in the troposphere, the R between retrieved tropospheric NO partial columns and stratospheric NO partial columns is only 0.11, indicating that there is no linear relationship between the retrieved tropospheric and stratospheric partial columns, and the retrieved tropospheric and stratospheric partial columns are almost independent.

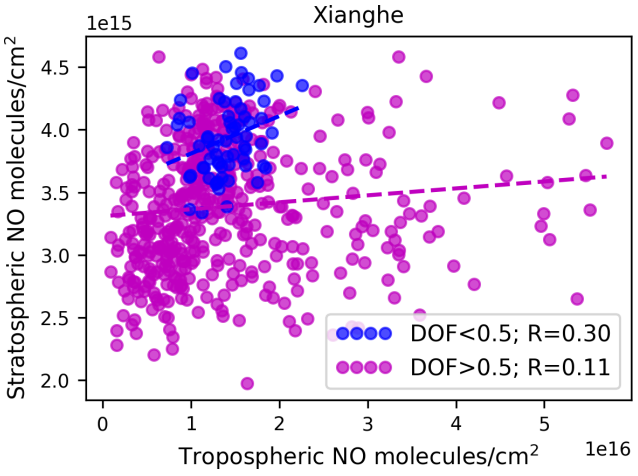

Figure 10. Scatterplots at Xianghe between the tropospheric NO partial columns and stratospheric NO partial columns with the DOF less than 0.5 (blue) and greater than 0.5 (magenta) in the troposphere. R is the correlation coefficient. Only the results at Xianghe are presented here as there is no retrieval with a DOF larger than 0.5 in the troposphere at Maïdo.

When the DOF is less than 0.5 in the troposphere, the R between retrieved tropospheric NO partial columns and stratospheric NO partial columns is slightly larger ($R = 0.30$). The reason for this increased correlation is that the retrieved tropospheric partial column is sensitive to the stratosphere, and the individual averaging kernels become broader.

Figure 11 shows the time series of the tropospheric NO partial columns at Xianghe. There is no tropospheric NO measurement in summer due to the high water vapor columns (Fig. 5). In addition, due to the COVID-19 lockdown, FTIR NO measurements are not available between 17 February and 23 May 2020. The mean (including SD) of the tropospheric NO partial columns is $1.4 \pm 1.0 \times 10^{16}$ molecules cm^{-2} at Xianghe. The low NO partial column is close to 0, and the high value can reach up to 5.8×10^{16} molecules cm^{-2}. There is no clear diurnal variation in the tropospheric NO partial columns derived from the FTIR measurements, but there is a large day-to-day variation in NO tropospheric partial columns, especially in winter. The NO partial column during November 2019–February 2020 is generally lower than that in the previous year. It is found that the FTIR tropospheric NO partial column during the COVID-19 lockdown is much less than that before the lockdown. Moreover, the mean FTIR tropospheric NO partial column between 24 January and 16 February in 2020 is 6.1×10^{15} molecules cm^{-2}, which is less than the tropospheric NO partial column of 1.1×10^{16} molecules cm^{-2} during the same period in 2019. The decrease in tropospheric NO partial column during the COVID-19 lockdown period observed by FTIR measurements at Xianghe is generally consistent with the 25 %–33 % decrease in NO_2 column observed by TROPOMI and OMI satellite measurements (Bauwens et al., 2020) and the 28 %–48 % decrease in NO_2 surface concentration derived from the air pollution sites in Beijing (Wang et al., 2020).

As Xianghe is located in a polluted area, many species have the same anthropogenic sources. For example, both NO and carbon monoxide (CO) are emitted by combustion from manufacturing and road transportation (Crippa et al., 2018). The FTIR-observed spectra at Xianghe are used to retrieve CO following the method recommended by the NDACC IRWG (Zhou et al., 2019). The DOF of the retrieved CO profile is about 2.2, and there is independent information in the tropospheric CO partial column (Zhou et al., 2018). Figure 12 shows the correlation between the daily means of FTIR-retrieved CO and NO partial columns in the troposphere in winter at Xianghe. The large tropospheric CO and NO partial columns are observed simultaneously. The R is 0.70, indicating that the FTIR measurements can capture the tropospheric NO partial column variability on a synoptic scale.

Although NO and CO have common emission sources, they are very different species in terms of lifetime, chemistry, and transport. Therefore, we also compare the FTIR NO measurements with the ground-based multi-axis differential optical absorption spectroscopy (MAX-DOAS) NO_2 measurements in the troposphere at Xianghe. The MAX-DOAS instrument is operated at the same building as the FTIR instrument at Xianghe. The MAX-DOAS measurements can provide NO_2 partial columns in the lower troposphere (0–4 km). For more information about the MAX-DOAS NO_2 retrieval technique, we refer to Hendrick et al. (2014) and the references therein. Due to an instrument failure, there is no data between August 2018 and September 2019 for the MAX-DOAS measurements. Nevertheless, we collect all the co-located FTIR NO and MAX-DOAS NO_2 measurements. Figure 12 shows the correlation between the daily means of FTIR-retrieved NO and MAX-DOAS-retrieved NO_2 partial columns in the lower troposphere (0–4 km) at Xianghe, with the R of 0.86. A good agreement between the NO and NO_2 is observed, and it confirms that the FTIR-retrieved tropospheric partial columns are reliable.

5 Conclusions

In this study, the ground-based FTIR solar spectra at Xianghe and Maïdo are applied to retrieve NO using the SFIT4 algorithm, with a focus on the NO partial columns in the troposphere and stratosphere. Xianghe is a polluted site with a high NO mole fraction near the surface, while Maïdo is a background site with a very low NO mole fraction near the surface. The systematic and random uncertainties in the retrieved NO total column are estimated as 10.3 % and 13.5 % at Xianghe and 10.3 % and 4.2 % at Maïdo. The DOF of the retrieved NO profile is 2.3 ± 0.4 at Xianghe and 1.3 ± 0.1 at Maïdo. The systematic and random uncertainties in the retrieved NO partial columns at Xianghe are estimated as

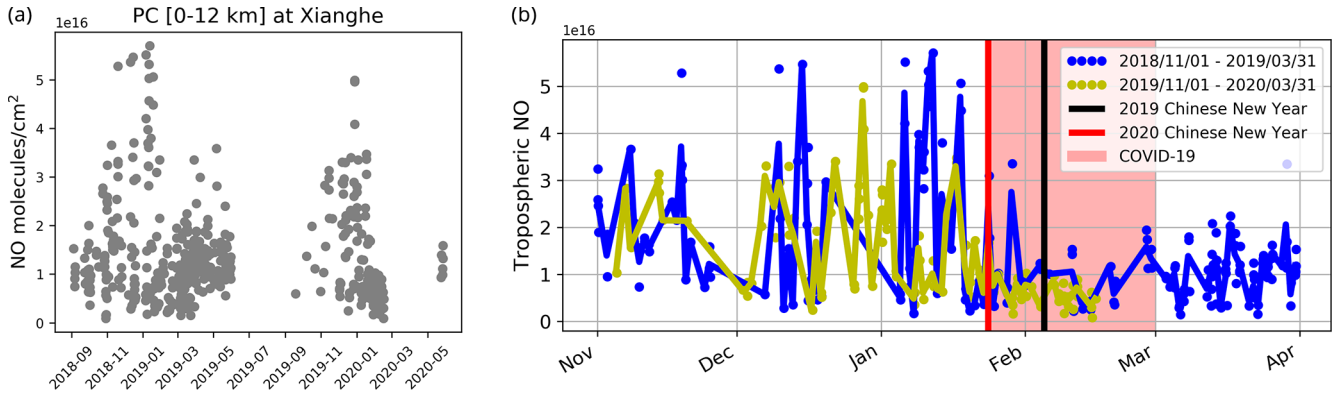

Figure 11. (a) The time series of the FTIR-retrieved tropospheric NO partial columns at Xianghe. **(b)** The time series of FTIR-retrieved tropospheric NO partial columns during November 2018–March 2019 and November 2019–March 2020. The blue and yellow dots are individual measurements, and the solid lines are daily means.

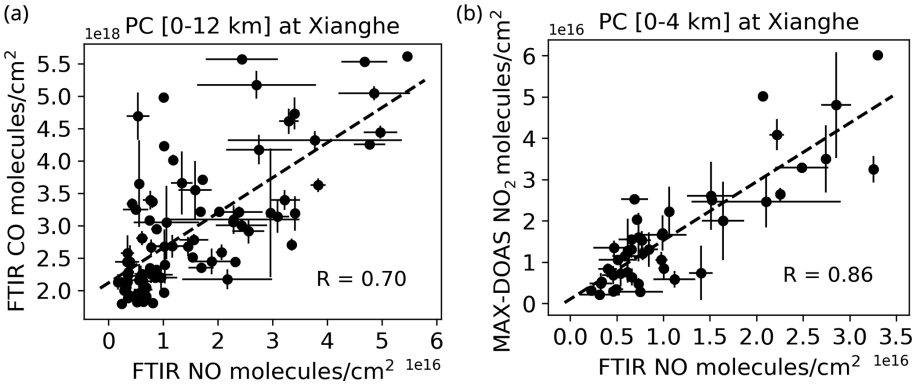

Figure 12. (a) The correlation between the daily means of the FTIR-retrieved NO tropospheric partial columns and the retrieved CO tropospheric partial columns in winter at Xianghe. **(b)** The correlation between the daily means of the FTIR-retrieved NO partial columns and MAX-DOAS-retrieved NO_2 partial columns between the surface and 4 km at Xianghe. The error bar is the daily SD, and the dashed black line is the linear fit.

10.5 % and 18.0 % in the troposphere and 10.2 % and 4.4 % in the stratosphere.

At both sites, we can obtain the NO partial column in the stratosphere from the FTIR retrievals. The FTIR retrievals are able to derive the diurnal variation in the NO partial column in the stratosphere during the daytime, especially at Maïdo. It is found that the stratospheric NO partial column increases with time in the morning to about 12:20 LT, and there is a linear relationship between the stratospheric NO partial column and the solar radiation intensity, with an R of 0.80 at Xianghe and 0.74 at Maïdo. The stratospheric NO partial column starts decreasing after about 14:00 LT at Maïdo, but at Xianghe it is hard to observe such consistent change in the stratospheric NO partial column after 14:00 LT due to the limited measurements. As there is a large diurnal variation in the stratospheric NO partial column, we use the measurements between 13:30 and 14:30 LT to derive the seasonal cycle of the stratospheric NO partial column. It is found that the phases of the seasonal variations in the stratospheric NO partial column at these two sites are similar, with a high value in local summer and a low value in local winter. Moreover, the FTIR NO partial columns in the stratosphere are compared with the MIPAS satellite observations. After taking the diurnal variation in NO into account, the stratospheric NO partial columns from co-located FTIR and MIPAS measurements show similar seasonal variations at both sites. Above Maïdo, the decrease rate observed by the MIPAS measurements between 2005 and 2012 is close to that observed by the FTIR measurements between 2013 and 2019. The systematic difference between the MIPAS and FTIR measurements is about 10 %, which is within their uncertainties.

The tropospheric NO partial column can be retrieved at the polluted site (Xianghe) but not at the background site (Maïdo). We select the retrieval with a DOF in the troposphere larger than 0.5 to calculate the tropospheric NO partial column. Since the SNR of the spectrum is highly dependent on the H_2O abundance, the successfully retrieved

tropospheric NO is generally under a dry condition with an H_2O total column less than 5.7×10^{22} molecules cm^{-2} at Xianghe. As a result, the tropospheric NO partial column is very difficult to retrieve in summer. The mean and SD of the tropospheric NO partial columns at Xianghe are $1.4 \pm 1.0 \times 10^{16}$ molecules cm^{-2}. The mean FTIR tropospheric NO partial column during the COVID-19 lockdown in 2020 is lower than that before the lockdown period and also lower than that during the same period in 2019. Large tropospheric NO_2 (or CO) and NO partial columns are observed simultaneously, indicating that the synoptic variation in the tropospheric NO partial columns can be well captured from the FTIR retrievals at Xianghe. It is the first study of a successful analysis of NO in the troposphere from a ground-based FTIR site. The tropospheric and stratospheric NO retrieval might be possible at other potential FTIR sites inside or near large cities with enhanced levels of NO near the surface.

Data availability. The MIPAS data are publicly available at https://www.imk-asf.kit.edu/english/308.php (last access: 6 September 2021, KIT MIPAS team, 2021). The FTIR NO retrievals at Xianghe and Maïdo are available upon request to the authors.

Author contributions. MZ wrote the manuscript. MZ and MDM designed the experiment. MZ, BD, and EM discussed the conceptualization. CH, NK, JMM, and PW collected the FTIR measurements at Xianghe and Maïdo. BL and CV investigated the FTIR retrieval strategy. All the authors read and commented on the manuscript.

Competing interests. The contact author has declared that neither they nor their co-authors have any competing interests.

Disclaimer. Publisher's note: Copernicus Publications remains neutral with regard to jurisdictional claims in published maps and institutional affiliations.

Acknowledgements. The authors would like to thank Rebecca Buchholz (NCAR) for providing the CAM-Chem model data and Francois Hendrick (BIRA-IASB) for providing the MAX-DOAS NO_2 measurements. EM is a senior research associate with the F.R.S. – FNRS (Brussels, Belgium).

Financial support. This FTIR measurements at Xianghe are funded by the National Natural Science Foundation of China (grant no. 41975035). The FTIR site at Reunion Island is operated by the BIRA-IASB and locally supported by LACy/UMR8105, Université de La Réunion.

Review statement. This paper was edited by Frank Hase and reviewed by two anonymous referees.

References

Bauwens, M., Compernolle, S., Stavrakou, T., Müller, J.-F., van Gent, J., Eskes, H., Levelt, P. F., van der A, R., Veefkind, J. P., Vlietinck, J., Yu, H., and Zehner, C.: Impact of Coronavirus Outbreak on NO_2 Pollution Assessed Using TROPOMI and OMI Observations, Geophys. Res. Lett., 47, e2020GL087 978, https://doi.org/10.1029/2020GL087978, 2020.

Bermejo-Pantaleón, D., Funke, B., López-Puertas, M., García-Comas, M., Stiller, G. P., von Clarmann, T., Linden, A., Grabowski, U., Höpfner, M., Kiefer, M., Glatthor, N., Kellmann, S., and Lu, G.: Global observations of thermospheric temperature and nitric oxide from MIPAS spectra at 5.3 µm, J. Geophys. Res.-Space, 116, A10313, https://doi.org/10.1029/2011JA016752, 2011.

Bernath, P. F., McElroy, C. T., Abrams, M. C., Boone, C. D., Butler, M., Camy-Peyret, C., Carleer, M., Clerbaux, C., Coheur, P. F., Colin, R., DeCola, P., DeMazière, M., Drummond, J. R., Dufour, D., Evans, W. F. J., Fast, H., Fussen, D., Gilbert, K., Jennings, D. E., Llewellyn, E. J., Lowe, R. P., Mahieu, E., McConnell, J. C., McHugh, M., McLeod, S. D., Michaud, R., Midwinter, C., Nassar, R., Nichitiu, F., Nowlan, C., Rinsland, C. P., Rochon, Y. J., Rowlands, N., Semeniuk, K., Simon, P., Skelton, R., Sloan, J. J., Soucy, M. A., Strong, K., Tremblay, P., Turnbull, D., Walker, K. A., Walkty, I., Wardle, D. A., Wehrle, V., Zander, R., and Zou, J.: Atmospheric chemistry experiment (ACE): Mission overview, Geophys. Res. Lett., 32, L15S01, https://doi.org/10.1029/2005GL022386, 2005.

Blumenstock, T., Hase, F., Keens, A., Czurlok, D., Colebatch, O., Garcia, O., Griffith, D. W. T., Grutter, M., Hannigan, J. W., Heikkinen, P., Jeseck, P., Jones, N., Kivi, R., Lutsch, E., Makarova, M., Imhasin, H. K., Mellqvist, J., Morino, I., Nagahama, T., Notholt, J., Ortega, I., Palm, M., Raffalski, U., Rettinger, M., Robinson, J., Schneider, M., Servais, C., Smale, D., Stremme, W., Strong, K., Sussmann, R., Té, Y., and Velazco, V. A.: Characterization and potential for reducing optical resonances in Fourier transform infrared spectrometers of the Network for the Detection of Atmospheric Composition Change (NDACC), Atmos. Meas. Tech., 14, 1239–1252, https://doi.org/10.5194/amt-14-1239-2021, 2021.

Crippa, M., Guizzardi, D., Muntean, M., Schaaf, E., Dentener, F., van Aardenne, J. A., Monni, S., Doering, U., Olivier, J. G. J., Pagliari, V., and Janssens-Maenhout, G.: Gridded emissions of air pollutants for the period 1970–2012 within EDGAR v4.3.2, Earth Syst. Sci. Data, 10, 1987–2013, https://doi.org/10.5194/essd-10-1987-2018, 2018.

Crutzen, P. J.: The influence of nitrogen oxides on the atmospheric ozone content, Q. J. Roy. Meteor. Soc., 96, 320–325, https://doi.org/10.1002/qj.49709640815, 1970.

Crutzen, P. J.: The Role of NO and NO_2 in the Chemistry of the Troposphere and Stratosphere, Annu. Rev. Earth Pl. Sc., 7, 443–472, https://doi.org/10.1146/annurev.ea.07.050179.002303, 1979.

Delmas, R., Serça, D., and Jambert, C.: Global inventory of NO_x sources, Nutr. Cycl. Agroecosys., 48, 51–60, https://doi.org/10.1023/A:1009793806086, 1997.

De Mazière, M., Thompson, A. M., Kurylo, M. J., Wild, J. D., Bernhard, G., Blumenstock, T., Braathen, G. O., Hannigan, J. W., Lambert, J.-C., Leblanc, T., McGee, T. J., Nedoluha, G., Petropavlovskikh, I., Seckmeyer, G., Simon, P. C., Steinbrecht, W., and Strahan, S. E.: The Network for the Detec-

tion of Atmospheric Composition Change (NDACC): history, status and perspectives, Atmos. Chem. Phys., 18, 4935–4964, https://doi.org/10.5194/acp-18-4935-2018, 2018.

Dubé, K., Randel, W., Bourassa, A., Zawada, D., McLinden, C., and Degenstein, D.: Trends and Variability in Stratospheric NO_x Derived From Merged SAGE II and OSIRIS Satellite Observations, J. Geophys. Res.-Atmos., 125, e2019JD031 798, https://doi.org/10.1029/2019JD031798, 2020.

Fischer, H., Birk, M., Blom, C., Carli, B., Carlotti, M., von Clarmann, T., Delbouille, L., Dudhia, A., Ehhalt, D., Endemann, M., Flaud, J. M., Gessner, R., Kleinert, A., Koopman, R., Langen, J., López-Puertas, M., Mosner, P., Nett, H., Oelhaf, H., Perron, G., Remedios, J., Ridolfi, M., Stiller, G., and Zander, R.: MIPAS: an instrument for atmospheric and climate research, Atmos. Chem. Phys., 8, 2151–2188, https://doi.org/10.5194/acp-8-2151-2008, 2008.

Galytska, E., Rozanov, A., Chipperfield, M. P., Dhomse, Sandip. S., Weber, M., Arosio, C., Feng, W., and Burrows, J. P.: Dynamically controlled ozone decline in the tropical mid-stratosphere observed by SCIAMACHY, Atmos. Chem. Phys., 19, 767–783, https://doi.org/10.5194/acp-19-767-2019, 2019.

Gordon, I., Rothman, L., Hill, C., Kochanov, R., Tan, Y., Bernath, P., Birk, M., Boudon, V., Campargue, A., Chance, K., Drouin, B., Flaud, J.-M., Gamache, R., Hodges, J., Jacquemart, D., Perevalov, V., Perrin, A., Shine, K., Smith, M.-A., Tennyson, J., Toon, G., Tran, H., Tyuterev, V., Barbe, A., Császár, A., Devi, V., Furtenbacher, T., Harrison, J., Hartmann, J.-M., Jolly, A., Johnson, T., Karman, T., Kleiner, I., Kyuberis, A., Loos, J., Lyulin, O., Massie, S., Mikhailenko, S., Moazzen-Ahmadi, N., Müller, H., Naumenko, O., Nikitin, A., Polyansky, O., Rey, M., Rotger, M., Sharpe, S., Sung, K., Starikova, E., Tashkun, S., Auwera, J. V., Wagner, G., Wilzewski, J., Wcisło, P., Yu, S., and Zak, E.: The HITRAN2016 molecular spectroscopic database, J. Quant. Spectrosc. Ra., 203, 3–69, https://doi.org/10.1016/j.jqsrt.2017.06.038, hITRAN2016 Special Issue, 2017.

Hase, F., Blumenstock, T., and Paton-Walsh, C.: Analysis of the Instrumental Line Shape of High-Resolution Fourier Transform IR Spectrometers with Gas Cell Measurements and New Retrieval Software, Appl. Opt., 38, 3417, https://doi.org/10.1364/AO.38.003417, 1999.

Hendrick, F., Müller, J.-F., Clémer, K., Wang, P., De Mazière, M., Fayt, C., Gielen, C., Hermans, C., Ma, J. Z., Pinardi, G., Stavrakou, T., Vlemmix, T., and Van Roozendael, M.: Four years of ground-based MAX-DOAS observations of HONO and NO_2 in the Beijing area, Atmos. Chem. Phys., 14, 765–781, https://doi.org/10.5194/acp-14-765-2014, 2014.

Jacob, D. J.: Introduction to Atmospheric Chemistry, Princeton University Press, Princeton, New Jersey, available at: http://www.jstor.org/stable/j.ctt7t8hg (last access: 8 September 2021), 1999.

Kalnay, E., Kanamitsu, M., Kistler, R., Collins, W., Deaven, D., Gandin, L., Iredell, M., Saha, S., White, G., Woollen, J., Zhu, Y., Chelliah, M., Ebisuzaki, W., Higgins, W., Janowiak, J., Mo, K. C., Ropelewski, C., Wang, J., Leetmaa, A., Reynolds, R., Jenne, R., and Joseph, D.: The NCEP/NCAR 40-Year Reanalysis Project, B. Am. Meteorol. Soc., 77, 437–472, https://doi.org/10.1175/1520-0477(1996)077<0437:TNYRP>2.0.CO;2, 1996.

KIT MIPAS team: MIPAS satellite datasets, KIT [data set], available at: https://www.imk-asf.kit.edu/english/308.php, last access: 6 September 2021.

Kondo, Y., Aimedieu, P., Pirre, M., Matthews, W. A., Ramaroson, R., Sheldon, W. R., Benbrook, J. R., and Iwata, A.: Diurnal variation of nitric oxide in the upper stratosphere, J. Geophys. Res.-Atmos., 95, 22513–22522, https://doi.org/10.1029/JD095iD13p22513, 1990.

Lamarque, J.-F., Emmons, L. K., Hess, P. G., Kinnison, D. E., Tilmes, S., Vitt, F., Heald, C. L., Holland, E. A., Lauritzen, P. H., Neu, J., Orlando, J. J., Rasch, P. J., and Tyndall, G. K.: CAM-chem: description and evaluation of interactive atmospheric chemistry in the Community Earth System Model, Geosci. Model Dev., 5, 369–411, https://doi.org/10.5194/gmd-5-369-2012, 2012.

Marsh, D. R., Mills, M. J., Kinnison, D. E., Lamarque, J.-F., Calvo, N., and Polvani, L. M.: Climate Change from 1850 to 2005 Simulated in CESM1(WACCM), J. Climate, 26, 7372–7391, https://doi.org/10.1175/JCLI-D-12-00558.1, 2013.

Meraner, K. and Schmidt, H.: Transport of nitrogen oxides through the winter mesopause in HAMMONIA, J. Geophys. Res.-Atmos., 121, 2556–2570, https://doi.org/10.1002/2015JD024136, 2016.

Monks, P. S., Archibald, A. T., Colette, A., Cooper, O., Coyle, M., Derwent, R., Fowler, D., Granier, C., Law, K. S., Mills, G. E., Stevenson, D. S., Tarasova, O., Thouret, V., von Schneidemesser, E., Sommariva, R., Wild, O., and Williams, M. L.: Tropospheric ozone and its precursors from the urban to the global scale from air quality to short-lived climate forcer, Atmos. Chem. Phys., 15, 8889–8973, https://doi.org/10.5194/acp-15-8889-2015, 2015.

Ng, N. L., Chhabra, P. S., Chan, A. W. H., Surratt, J. D., Kroll, J. H., Kwan, A. J., McCabe, D. C., Wennberg, P. O., Sorooshian, A., Murphy, S. M., Dalleska, N. F., Flagan, R. C., and Seinfeld, J. H.: Effect of NO_x level on secondary organic aerosol (SOA) formation from the photooxidation of terpenes, Atmos. Chem. Phys., 7, 5159–5174, https://doi.org/10.5194/acp-7-5159-2007, 2007.

Notholt, J., Meier, A., and Peil, S.: Total column densities of tropospheric and stratospheric trace gases in the undisturbed Arctic summer atmosphere, J. Atmos. Chem., 20, 311–332, https://doi.org/10.1007/BF00694500, 1995.

Park, S., Croteau, P., Boering, K. A., Etheridge, D. M., Ferretti, D., Fraser, P. J., Kim, K. R., Krummel, P. B., Langenfelds, R. L., Van Ommen, T. D., Steele, L. P., and Trudinger, C. M.: Trends and seasonal cycles in the isotopic composition of nitrous oxide since 1940, Nat. Geosci., 5, 261–265, https://doi.org/10.1038/ngeo1421, 2012.

Portmann, R. W., Daniel, J. S., and Ravishankara, A. R.: Stratospheric ozone depletion due to nitrous oxide: influences of other gases, Philos. T. R. Soc. B, 367, 1256–1264, https://doi.org/10.1098/rstb.2011.0377, 2012.

Pougatchev, N. S., Connor, B. J., and Rinsland, C. P.: Infrared measurements of the ozone vertical distribution above Kitt Peak, J. Geophys. Res., 100, 16 689, https://doi.org/10.1029/95JD01296, 1995.

Randall, C. E., Harvey, V. L., Singleton, C. S., Bailey, S. M., Bernath, P. F., Codrescu, M., Nakajima, H., and Russell III, J. M.: Energetic particle precipitation effects on the Southern Hemisphere stratosphere in 1992–2005, J. Geophys. Res.-Atmos., 112, D08308, https://doi.org/10.1029/2006JD007696, 2007.

Rocco, M., Colomb, A., Baray, J.-L., Amelynck, C., Verreyken, B., Borbon, A., Pichon, J.-M., Bouvier, L., Schoon, N., Gros, V., Sarda-Esteve, R., Tulet, P., Metzger, J.-M., Duflot, V., Guadagno, C., Peris, G., and Brioude, J.: Analysis of Volatile Organic Compounds during the OCTAVE Campaign: Sources and Distributions of Formaldehyde on Reunion Island, Atmosphere, 11, 140, https://doi.org/10.3390/atmos11020140, 2020.

Rodgers, C. D.: Inverse Methods for Atmospheric Sounding – Theory and Practice, Series on Atmospheric Oceanic and Planetary Physics, 2, World Scientific Publishing Co. Pte. Ltd, Singapore, https://doi.org/10.1142/9789812813718, 2000.

Rodgers, C. D. and Connor, B. J.: Intercomparison of remote sounding instruments, J. Geophys. Res., 108, 46–48, https://doi.org/10.1029/2002JD002299, 2003.

Sheese, P. E., Walker, K. A., Boone, C. D., McLinden, C. A., Bernath, P. F., Bourassa, A. E., Burrows, J. P., Degenstein, D. A., Funke, B., Fussen, D., Manney, G. L., McElroy, C. T., Murtagh, D., Randall, C. E., Raspollini, P., Rozanov, A., Russell III, J. M., Suzuki, M., Shiotani, M., Urban, J., von Clarmann, T., and Zawodny, J. M.: Validation of ACE-FTS version 3.5 NO_y species profiles using correlative satellite measurements, Atmos. Meas. Tech., 9, 5781–5810, https://doi.org/10.5194/amt-9-5781-2016, 2016.

Steck, T.: Methods for determining regularization for atmospheric retrieval problems, Appl. Opt., 41, 1788–1797, https://doi.org/10.1364/AO.41.001788, 2002.

Tang, G., Li, X., Wang, Y., Xin, J., and Ren, X.: Surface ozone trend details and interpretations in Beijing, 2001–2006, Atmos. Chem. Phys., 9, 8813–8823, https://doi.org/10.5194/acp-9-8813-2009, 2009.

Tikhonov, A. N.: Solution of Incorrectly Formulated Problems and the Regularisation Method, Soviet. Math. Dokl., 4, 1035–1038, 1963.

Vaughan, G., Quinn, P. T., Green, A. C., Bean, J., Roscoe, H. K., van Roozendael, M., and Goutail, F.: SAOZ measurements of NO_2 at Aberystwyth, J. Environ. Monitor., 8, 353–361, https://doi.org/10.1039/B511482A, 2006.

Wang, Y., Wen, Y., Wang, Y., Zhang, S., Zhang, K. M., Zheng, H., Xing, J., Wu, Y., and Hao, J.: Four-Month Changes in Air Quality during and after the COVID-19 Lockdown in Six Megacities in China, Environ. Sci. Technol. Lett., 7, 802–808, https://doi.org/10.1021/acs.estlett.0c00605, 2020.

Wiacek, A., Jones, N. B., Strong, K., Taylor, J. R., Mittermeier, R. L., and Fast, H.: First detection of mesothermospheric Nitric Oxide (NO) by ground-based FTIR solar absorption spectroscopy, Geophys. Res. Lett., 33, L03811, https://doi.org/10.1029/2005GL024897, 2006.

Yang, Y., Zhou, M., Langerock, B., Sha, M. K., Hermans, C., Wang, T., Ji, D., Vigouroux, C., Kumps, N., Wang, G., De Mazière, M., and Wang, P.: New ground-based Fourier-transform near-infrared solar absorption measurements of XCO_2, XCH_4 and XCO at Xianghe, China, Earth Syst. Sci. Data, 12, 1679–1696, https://doi.org/10.5194/essd-12-1679-2020, 2020.

Zhou, M., Vigouroux, C., Langerock, B., Wang, P., Dutton, G., Hermans, C., Kumps, N., Metzger, J.-M., Toon, G., and De Mazière, M.: CFC-11, CFC-12 and HCFC-22 ground-based remote sensing FTIR measurements at Réunion Island and comparisons with MIPAS/ENVISAT data, Atmos. Meas. Tech., 9, 5621–5636, https://doi.org/10.5194/amt-9-5621-2016, 2016.

Zhou, M., Langerock, B., Vigouroux, C., Sha, M. K., Ramonet, M., Delmotte, M., Mahieu, E., Bader, W., Hermans, C., Kumps, N., Metzger, J.-M., Duflot, V., Wang, Z., Palm, M., and De Mazière, M.: Atmospheric CO and CH_4 time series and seasonal variations on Reunion Island from ground-based in situ and FTIR (NDACC and TCCON) measurements, Atmos. Chem. Phys., 18, 13881–13901, https://doi.org/10.5194/acp-18-13881-2018, 2018.

Zhou, M., Langerock, B., Vigouroux, C., Sha, M. K., Hermans, C., Metzger, J.-M., Chen, H., Ramonet, M., Kivi, R., Heikkinen, P., Smale, D., Pollard, D. F., Jones, N., Velazco, V. A., García, O. E., Schneider, M., Palm, M., Warneke, T., and De Mazière, M.: TCCON and NDACC X_{CO} measurements: difference, discussion and application, Atmos. Meas. Tech., 12, 5979–5995, https://doi.org/10.5194/amt-12-5979-2019, 2019.

Zhou, M., Wang, P., Langerock, B., Vigouroux, C., Hermans, C., Kumps, N., Wang, T., Yang, Y., Ji, D., Ran, L., Zhang, J., Xuan, Y., Chen, H., Posny, F., Duflot, V., Metzger, J.-M., and De Mazière, M.: Ground-based Fourier transform infrared (FTIR) O_3 retrievals from the 3040 cm^{-1} spectral range at Xianghe, China, Atmos. Meas. Tech., 13, 5379–5394, https://doi.org/10.5194/amt-13-5379-2020, 2020.